Surface electron motion near monatomic steps: Two-photon photoemission studies on stepped Cu(111)

X. Y. Wang, X. J. Shen, and R. M. Osgood, Jr.
Columbia Radiation Laboratory, Columbia University, New York, New York 10027
(Received 8 May 1997)

The electronic structure of three surface or near-surface states on stepped Cu(775) has been investigated using angle-resolved, resonant, two-photon photoemission. Since the electron wave function in each of these electronic states has a different average distance from the crystal plane, the measurement allowed the step potential at each distance to be sampled. The energy dispersion of the $n=1$ image-potential state was found to be oriented by the (111) terrace and the $n=2$ state was oriented by the (775) surface plane. The band structure of the embedded sp-like surface state ($n=0$) was determined by the projection of the bulk band gap onto Cu(775). [S0163-1829(97)05635-X]

I. INTRODUCTION

The electronic structure near or at stepped surfaces, has recently attracted considerable attention[1–8] because of its relevance to the physics of nanoscale surface features. For example, well-defined stepped surfaces can offer simple structures of atomic scale for examining electronic phenomena; on certain vicinal surfaces uniform arrays of monatomic step heights can be arranged with spacings of only tens of angstroms. The understanding of the scattering of confined electrons at discontinuities on metal surfaces has recently been the focus of a lively series of experimental and theoretical investigations. For example, scanning tunneling microscopy (STM) studies have shown electron standing-wave phenomena involving electrons in the sp surface state scattering from isolated step structures as well as from adsorbed atoms.[1–4] The contrast in the images of these surface waves at different sample voltages is sufficient that mapping of their dispersive properties has been reported.[2] In addition, STM spectroscopy has shown binding-energy shifts of surface electrons on vicinal copper surfaces which were attributed to lateral confinement by surface steps.[7] Finally, artificial structures, e.g., ''quantum corrals,'' have been assembled in order to examine electron confinement within their periphery.[1] A recent theoretical study has pointed out that scattering of surface-state electrons within the corrals into the bulk may provide an important ''loss'' term which could greatly reduce the confinement efficiency of the atom barriers.[5]

This recent work using proximal probes may be compared to the results of studies of surface electronic structure using photoemission. For example, there have been several angle-resolved photoelectron spectroscopic measurements of sp-like surface states[7,9–11] as well as valence-band structures[12] at stepped surfaces. These stepped surfaces were typically formed by making small-angle miscuts to the (111) plane of noble metal crystals. In these studies the dispersion minima of the surface states were found to be determined by the projected bulk band structure on the surface Brillouin zone (SBZ) and to be significantly different from that of flat Cu(111). The results thus indicated that these surface states are largely delocalized in the surface plane and the lateral coherence length is larger than the terrace width.[11]

Unoccupied-state spectroscopy has shown, initially using inverse photoemission,[13] a close relationship between these crystal-induced sp states and the surface Rydberg or image states on flat surfaces of a single-crystal metal. Each case can be treated as a two-dimensional (2D) free-electron-like system. However, electrons in image states are confined *above* the surface, instead of beneath the surface in the case of the crystal-induced states, by the Coulombic force of the image charge polarized in the surface.[14] In the absence of any lateral confinement potential, image-state electrons move freely in a plane parallel to the surface. Image electrons are somewhat decoupled from the bulk and only interact weakly with the bulk crystal due to the crystal barrier, but interact more strongly with surface imperfections or impurities. Such coupling to surface features may be manifest either in the form of binding-energy shifts or broadening of the image-state kinetic-energy distribution.[8,15]

As a result, it is of interest to determine how image electrons may interact with the surface potential of steps on a single-crystal metal surface. The use of image-state photoemission provides several interesting possibilities for probing this system. First, these surface or near-surface electrons can have very narrow photoemission linewidths, thus allowing small shifts, i.e., ~tens of meV, to be observed. Second, by examining electrons in states with different principal quantum numbers,[14] it is possible to examine electron lateral motion at different distances, on average, from the crystal plane. The use of angle-resolved photoemission provides complementary information on surface-electron scattering from that obtained in STM studies, since in the case of the former, momentum-resolved measurements allow the surface electronic structure, i.e., energy versus the electron wave vector, to be mapped throughout the surface Brillouin zone.

Specifically, in this paper we present comparative studies of the electronic behavior of surface electrons in both crystal-and image-induced states on a single-crystal vicinal surface and the relevant flat low-Miller-index surface. Our measurements use angle-resolved, *resonant*, two-photon photoemission, a technique which allowed simultaneous probing of a set of occupied and unoccupied bands. With this technique, we have investigated the local electronic proper-

ties of the $n=0$ sp-like surface state,[16,17] and $n=1$ and 2 image states[18] on flat Cu(111) and stepped Cu(775). Because these states exist at different average distances with respect to the surface plane, in effect, the electron lateral motion was studied as a function of height from the stepped surface. The step array on vicinal Cu(775) can be very uniform, thus the use of this surface should also allow coherent scattering from an array of monatomic steps to be probed as well.

Recent studies have shown that two-photon photoemission (2PPE) spectroscopy is a very sensitive and nonperturbative tool for investigating a variety of image-electron physical phenomena on many metallic surfaces.[19] In this method, a photon first populates the image state from an occupied electronic state below the Fermi level and the image state is then probed with a second photon by photoionizing the image-state electron. For a fixed initial surface state, probing of the image states can be accomplished through resonant excitation with a proper photon energy.[20] Because of the relatively large overlap of the two wave functions for the initial and intermediate states the excitation process is very efficient. Earlier experiments with resonant 2PPE technique have generally used excitation with a fixed photon energy or photoemission detection at a fixed angle. In the measurements presented here, angle-resolved resonant as well as off-resonant bichromatic or monochromatic two-photon photoemission were employed. By tuning the photon energy of nanosecond laser pulses *and* the detection angle, resonant two-photon excitation from the sp surface state ($n=0$) to the image-potential states ($n=1,2$) can be achieved at various electron momenta ($k_{\parallel}$) parallel to the surface and hence the energy bands of both the initial and intermediate states can be mapped out directly. This approach has recently been reported for simultaneous measurement of the $n=0$ surface resonance and the $n=1$ state on Ni(111).[20]

The goal of the experiments described in this paper has been to investigate the motion of electrons on a well-prepared stepped surface and to determine the confinement of the electron by a series of step-edge potentials at room temperature. The measurements display distinct dispersion minima as well as different binding-energy shifts for the three surface states, each of them located at a different distance from the surface. The results show that the $n=1$ image state, located about 2–3 Å above the surface, is most strongly coupled with the step structure.

The outline of this paper is as follows: The details of the experimental technique as well as the sample preparation are given in Sec. II. The experimental data using angle-resolved resonant 2PPE are presented and the energy bands of $n=0$, 1, and 2 states on vicinal Cu(775) are derived in Sec. III. Section IV discusses the shifts of the dispersion curve as well as the changes in the binding energy of these states on Cu(775) in comparison to those on flat Cu(111). Finally, the major findings and implications for further experiments are summarized in Sec. V.

II. EXPERIMENT

A high-purity single-crystal sample was spark-cut from a Cu(111) boule (99.999% purity) of 1.2-cm diameter. The stepped Cu(775) was formed by an 8.5° miscut to the Cu(111) surface (see Fig. 1), while the reverse side of the same crystal was cut to provide a flat Cu(111) surface. The sample was loosely held by the side and mounted onto two tungsten rods in an UHV chamber so that both the stepped and flat Cu(111) sides are accessible in the experimental configuration for angle-resolved measurements. Both surfaces were sequentially mechanically and electrochemically polished before being inserted into the UHV chamber, and then subjected to repeated sputter-anneal cycles until sharp low-evergy electron-diffraction (LEED) patterns were observed. With a carefully prepared crystal, the LEED spots exhibited sharp splitting, indicating a regular step morphology.[21] With an 8.5° miscut, monatomic steps would be expected to be formed along the $[1\bar{1}0]$ direction with the (111) terrace consisting of seven rows of $[1\bar{1}0]$-oriented atoms, corresponding to an intrinsic terrace width of $D_0=14.03$ Å. An analysis[21] of the LEED pattern gave a terrace width of $d=14\pm1$ Å, in good agreement with the expected value.

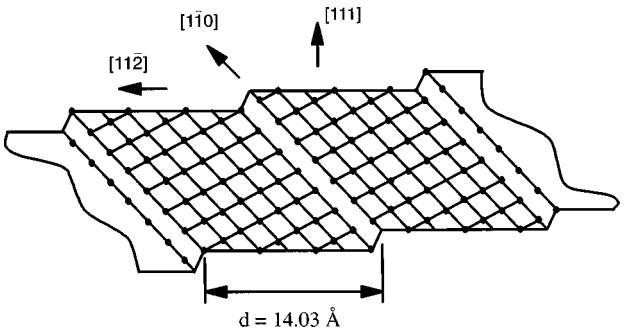

FIG. 1. A schematic diagram of an ideal lattice structure of Cu(775), or Cu(S)-[7(111)×(111)], showing (111) terraces of seven atomic rows separated by monatomic steps.

Photoemission experiments were performed with 17-ns, p-polarized laser pulses generated from a three-stage excimer-laser-pumped, tunable dye laser with the output radiation in the visible spectrum range. Frequency-doubled laser pulses with photon energies $2h\nu=4.2-4.9$ eV were used to populate the image states; the intensity of the incident light was kept low enough to avoid space-charge effects.[22] Detection and sample preparation was in a chamber kept at a base pressure $<2.0\times10^{-10}$ Torr during the measurement. The electron energy distribution was analyzed with an electrostatic, 160° (36.5-mm radius) spherical-sector analyzer. The acceptance cone of the detector is about 0.001 sr, giving a momentum resolution $\lesssim0.02$ Å^{-1} for the measurements presented here. The detector energy resolution was set at ~150 meV as a compromise for signal sensitivity and resolution. In the angle-resolved experiment, the laser incidence was *fixed* at 70° while the detector was rotated in a plane which is perpendicular to both the sample surface and the step direction, in most cases. This choice of the rotational axis for angle-resolved measurements allowed the interaction of the surface electron with the step structure to be probed; the accuracy of this rotation was better than ±0.2°. In this configuration, the excitation conditions, i.e., laser incidence and intensity, were always kept the same for each set of angle-resolved measurements; this procedure is important for resonant excitation experiments in which the signal intensity must be compared with data taken at other angular positions. The absolute angular position of the detector with respect to

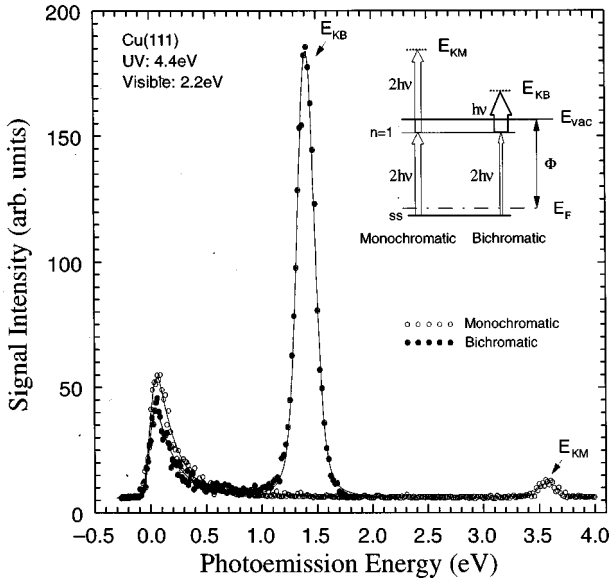

FIG. 2. Typical monochromatic and bichromatic 2PPE spectra on Cu(111) at fundamental wavelength $\lambda = 565$ nm.

the surface normal was determined optically with an accuracy better than $\pm 1°$.

In conventional 2PPE, UV light is used both for pumping electrons to the image states and for photoionizing the image-state electrons. In order to enhance the sensitivity of electron detection and eliminate space-charge effects due to intense 1PPE from the UV laser light, especially at higher photon energies, bichromatic 2PPE spectroscopy[23] was deployed for mapping the dispersion relations of the $n = 0$, 1, and 2 states. In bichromatic excitation a relatively weak UV intensity is used for the first excitation step while much more intense pulses of visible light are used to ionize the electrons (see Fig. 2). The visible light photon energy of $h\nu$ is not only well below the threshold level for single-photon photoemission but in addition has a three times larger photoemission cross section than for UV radiation at $2h\nu$ according to the wavelength-dependent expression for photoemission, given by Shakeshaft and Spruch.[24] The visible beam, which is originally *s*-polarized, and the *p*-polarized UV beam are directed through a visible broadband half-wave plate and a UV thin-film polarizer so that the UV and visible are collimated collinearly and are both *p* polarized when incident on the sample surface, thus allowing efficient excitation of surface states.

III. MAPPING OF THE ENERGY DISPERSION CURVES FOR THE $n = 0$, 1, 2 STATES

Both the *sp* surface state and image states on flat Cu(111) have been extensively studied using angle-resolved ultraviolet photoemission spectroscopy (Refs. 16 and 17) and angle-resolved 2PPE,[18] respectively. Figure 3 shows the well-known energy-band diagrams of the $n = 0$ (*sp*-like surface state[17]) and $n = 1$, 2 (image states[18]) on Cu(111), which were obtained from these measurements. In addition, the diagram depicts the resonant-excitation process, where the excitation is from the occupied $n = 0$ state to the unoccupied $n = 1$ or 2 states. Because the projected band gap near $k_{\|} \sim 0$ extends

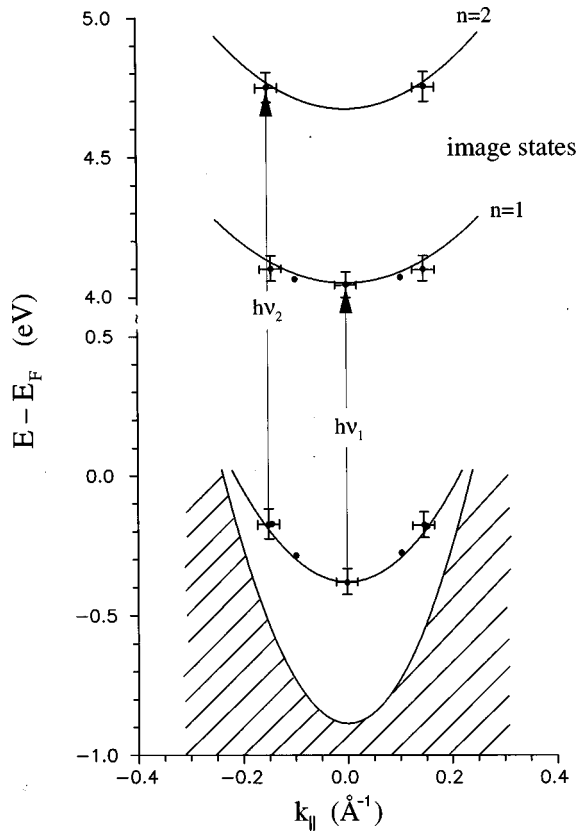

FIG. 3. Cu(111) energy-band diagram for the $n = 0$ to 1, 2 states, after Refs. 17 and 18. The shaded area is the bulk band. The closed circles are data obtained by our angle-resolved resonant 2PPE measurements.

from 0.9 eV below the Fermi level, E_F, to 4.1 eV above E_F, there is no occupied *bulk-state continuum* in the vicinity of the Fermi level at zone center, although the $n = 0$ surface state does lie in this same region of E-k space. In fact, at zone center a photon energy of at least 4.9 eV is required to excite electrons from the bulk continuum to the $n = 1$ image state. Thus, for the wavelengths used in the experiment, resonant excitation from the discrete surface state ($n = 0$, located ~ 0.4 eV below E_F at $k_{\|} = 0$) to the image states is the dominant excitation path for the two-photon signal. Such resonant excitation at a fixed photon energy only occurs for a narrow angular region around a specific initial value of $k_{\|}$. This method contrasts with excitation on many other metal surfaces, e.g., Cu(100), Ag(100), etc.,[25] which offer a continuum of occupied states up to the Fermi level and thus permit strong pumping of the image state over a broad range of photon energies, $h\nu \geq \Phi - E_B$, where Φ is the work function and E_B is the binding energy of the image state. In the case of resonant excitation with a discrete initial state, angle-resolved measurements at various $k_{\|}$ have to be accomplished via simultaneous tuning of the photon energy and detection angle. This procedure, while time consuming, does allow the energy bands of both the initial and intermediate states to be mapped simultaneously.

The $n = 1$ image state of Cu(111) has a binding energy which places it at the very top of the projected band gap at $k_{\|} = 0$; further the dispersion of the $n = 1$ state relative to that of the upper edge of the projected gap causes the $n = 1$ state

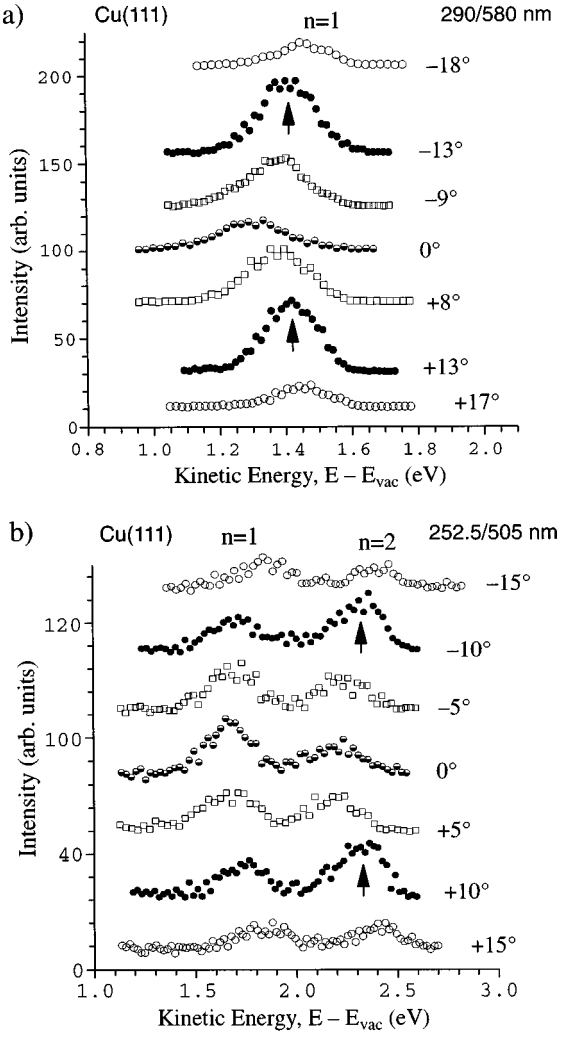

FIG. 4. Angle-resolved bichromatic 2PPE spectra on Cu(111): (a) at 290/580 nm; (b) at 252.5/505 nm.

to cross above the band gap immediately beyond $k_{\parallel}=0$.[16,26] Thus both the $n=1$ and 2 states are image resonances[27] for $k_{\parallel}>0$. Despite this, 2PPE measurements by Kubiak and others[18,26] have shown that both these image-state photoemission linewidths remain narrow and exhibit effective masses very close to the free-electron value. The narrow linewidths presumably reflect a low density of bulk states just beyond the projected band gap. Note that on flat Cu(111), the dispersion curves of all the three states are symmetric about the surface normal, or $k_{\parallel}=0$ in k space.

A. Results on Cu(111)

Since the energy bands of the surface electrons on Cu(111) had been well studied, angle-resolved resonant 2PPE measurements were first performed on this flat surface for reference and calibration. Figure 4(a) shows a set of angle-resolved 2PPE spectra taken using bichromatic excitation, with wavelengths of $\lambda_{\text{pump}}=290$ nm (frequency-doubled) and $\lambda_{\text{PE}}=580$ nm (fundamental) at detection angles from $-18°$ to $+17°$. Here, the minus sign on the angle was chosen to denote a direction from the surface normal [775] towards [112] in the plane perpendicular to the steps, while the positive sign applies to polar angles opposite from the surface normal. The $n=1$ state, identified by its well-defined binding energy,[18] was excited from the $n=0$ surface state. When using resonance excitation for band mapping both the initial and intermediate states can be tracked simultaneously. However, the technique requires that the resonance be identified by a maximum in signal intensity as the detection angle is varied.

As shown in Fig. 4(a) at the pump wavelength of 290 nm the maximum signal intensities of the $n=1$ state occurred at $+13°$ as well as $-13°$, but not in the surface normal direction, unlike the case on Cu(100). In addition, the spectra were symmetric about the normal, i.e., the $n=1$ signal had about the same intensity to within $\pm 5\%$ at the opposite $(\pm)$ angular position from the surface normal. Representative bichromatic 2PPE spectra taken at shorter excitation/photoemission wavelengths 252.5/505 nm are shown in Fig. 4(b), at this wavelength both the $n=1$ and 2 image states were excited and observed, as labeled in the figure. At each wavelength the $n=2$ peak was identified by the value of its binding energy.[18] These peaks were distinguished from a virtual 2PPE (Refs. 26 and 28) process involving the $n=0$ state by the disappearance of the feature as the pump wavelength was varied, see Fig. 4(a). Here, the $n=1$ state was populated from the upper edge of the bulk continuum, and the $n=2$ state was excited from the $n=0$ surface state. At these wavelengths the maximum intensities also occurred off $(\pm 10°)$ the normal for the $n=2$ state, and the spectra were again symmetric about the surface normal. Similar measurements at a series of other wavelengths showed that excitation at larger or lower photon energies resulted in resonance peaks at larger or smaller detection angles from the surface normal $(\theta=0°)$, with the spectra always being symmetric about $\theta=0°$. Such measurements also show that the excited electrons in image states do not relax to their band minima due to electron-electron interaction[29] within their lifetime, presumably a reflection of the weak image-electron interaction with the bulk-and surface-state electrons. In addition, the low density of electrons excited to the image states apparently prevents electron-electron thermalization.

Using data such as those shown in Fig. 4 at several wavelengths, the binding energies of both the initial and intermediate states could be tracked by measuring the angle, at which resonant excitation occurred, and the kinetic energy of the emitted electron for a given photon energy. Specifically, each resonant point reveals one point $(E,k_{\parallel})$ in the energy band of the image state as well as the sp surface state; the binding energy is given by $E_B=h\nu-E_{\text{kin}}$ (for $n=1$, or 2) relative to the vacuum level or $E_A=h\nu-\Phi+E_B$ relative to the Fermi level (for $n=0$), where E_{kin} is the kinetic energy of the photoemitted electron above the vacuum level. The lateral momentum $k_{\parallel}$ is conserved throughout the 2PPE process and is given by $k_{\parallel}=(\sqrt{2m_eE_{\text{kin}}}/\hbar)\sin\theta$. As shown in Fig. 3 the experimental results agree well, within the experimental error, with earlier measurements[17,18] for the $n=0$, 1, and 2 dispersion relations. The experimental error mainly stems from the finite signal-to-noise ratio of the system, possible remaining space-charge effects, the accuracy in the determination of the detection angle, and the detector energy and angular resolution.

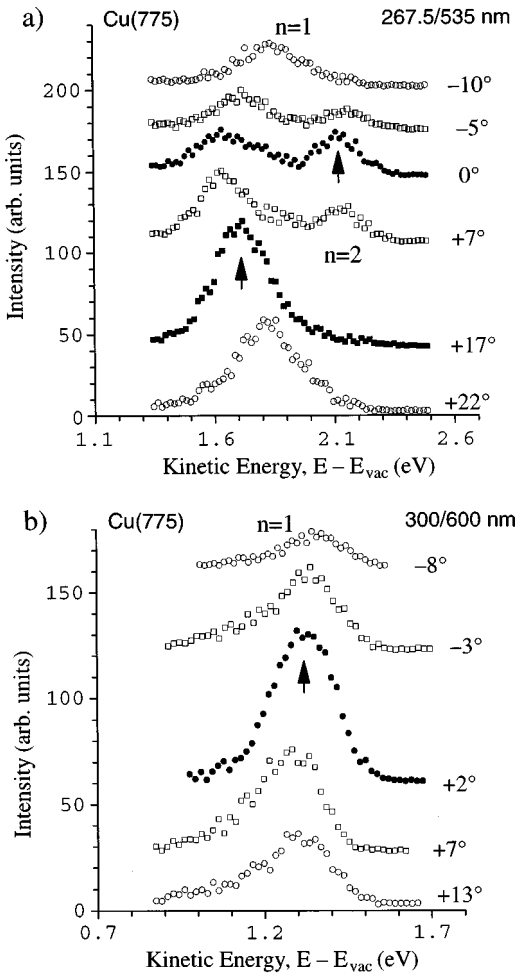

FIG. 5. Angle-resolved bichromatic 2PPE spectra on Cu(775): (a) at 267.5/535 nm; (b) at 300/600 nm.

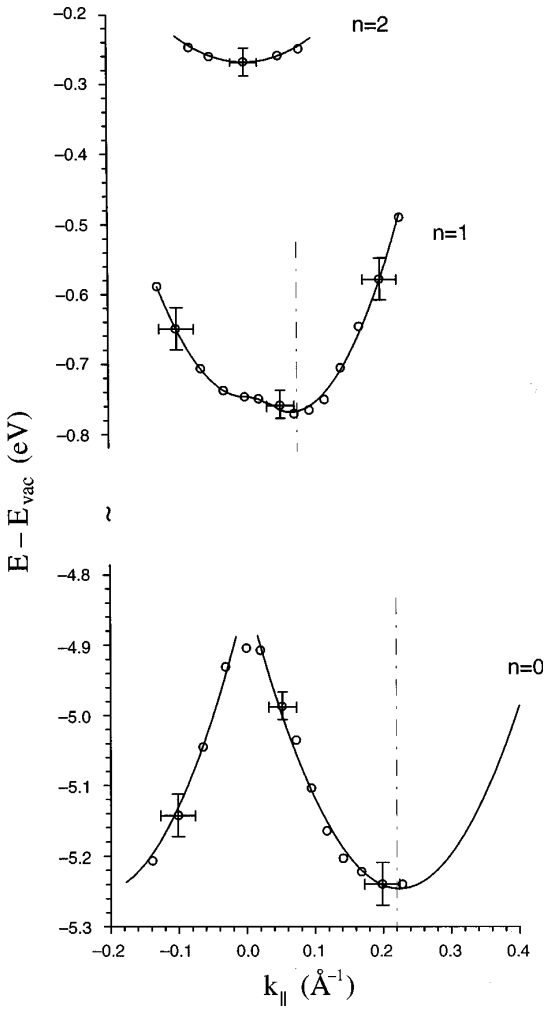

FIG. 6. Energy dispersion curves of the $n=0$, 1, and 2 states, determined by angle-resolved resonant 2PPE, on stepped Cu(775).

B. Results on Cu(775)

Angle-resolved, resonant, 2PPE measurements were then performed on carefully prepared stepped Cu(775). Figure 5(a) shows the 2PPE spectra on Cu(775) for detection angles $\theta=-10°$ to $+22°$ using bichromatic excitation at 267.5 and 535 nm. Both $n=1$ and 2 states were accessible from the $n=0$ state at this UV photon energy ($h\nu=4.64$ eV). As the detection scanned through various angular positions, only one resonance peak was observed for each image state, in contrast to the case on flat Cu(111). Specifically the resonance peaks are found at $\theta=+17°$ for the $n=1$ state and at $\theta=0°$ for the $n=2$ state. Thus the symmetry in the spectra for $\pm k_{\|}$ that was seen on the flat surface, was not present on the stepped surface, and the spectra were not symmetric about the surface normal or any other particular direction for either the $n=1$ or 2 state. As a second example, Fig. 5(b) shows a spectrum obtained for bichromatic excitation at somewhat longer wavelengths, e.g., 300 and 600 nm. The spectrum shows that only the $n=1$ state could be populated and that the resonance occurred at $\theta=+2°$. Again, there was only a single resonance peak and the symmetry about the surface normal, as seen on flat Cu(111), was again lost on Cu(775).

Further measurements at various photon energies and detection angles showed that for different photon energies, the signal intensity maxima appeared at different angles, which corresponded to different resonant-excitation positions in momentum space. At each resonant point, the binding energies of both the initial $n=0$ state and the intermediate image state at their corresponding momentum position can be simultaneously determined for the particular photon energy because of the fact that the parallel momentum is conserved during photoemission experiments, as described earlier in Sec. III A.

A plot of each value of E vs $k_{\|}$ corresponding to a particular resonance allowed the energy dispersion of the $n=0$, 1, and 2 states on Cu(775) to be mapped, as shown in Fig. 6. The binding energies of the image states, E_B, at a specific $k_{\|}$ value were determined from photon energy for *resonant excitation* at that $k_{\|}$, by the relation $E_B=h\nu_2-E_{\rm kin}$, where $E_{\rm kin}$ is the electron kinetic energy above the vacuum level and $h\nu_2$ is the photon energy for the photoionization step. Values of $E_{\rm kin}$ were determined from the energy-distribution curve (EDC) by measuring the position of the resonance peak relative to the low-energy cutoff in the 1PPE, a measure of the vacuum level. The EDC's in Figs. 4 and 5 were peak fit with a Voigt profile, which is a convolution of a Lorentzian line shape and the Gaussian response function of the detector. The binding energy of the $n=0$ surface state, E_B^0 was determined by the relation $E_B^0=E_B$

$+h\nu_1$, where $h\nu_1$ is the energy of the photon that excited the electron from $n=0$ to the image state at resonance. Figure 6 shows that the dispersion minima of both the $n=0$ and 1 states are shifted in k space, a result which contrasts with the nesting at about $k_{\|}=0$ for these same states on flat Cu(111). However, in the case of the $n=2$ state the dispersion curve was still centered at $k_{\|}=0$. The energy-band minimum of the $n=0$ state was found to be located at $k_{\|}\sim 0.22$ Å^{-1}, corresponding to a 19° detection angle for a probing photon energy ~2.36 eV. In the opposite direction from $k_{\|}=0$ ($\theta<0$, ''downhill'' on the steps), a second downward dispersion, which was symmetric to the above-mentioned dispersion in the ''uphill'' region, was also seen. Measurements at larger angles were not accessible in the downhill direction due to experimental constraints. Note that the resonant 2PPE signal was considerably weaker in comparison to that in the uphill direction.

The $n=1$ state minimum was shifted to $k_{\|}\sim 0.09$ Å^{-1}, or $\theta=8$–9°, an angle which corresponds to the direction along the terrace normal, i.e., [111]. Also note that this dispersion curve is not as symmetric about the dispersion minimum as that on flat Cu(111); in fact, there is an inflection point at $k_{\|}\sim 0$, whose existence was carefully verified repeatedly by both resonant excitation measurements and angle-resolved measurements at fixed photon energies close to the resonance.

These shifts in the dispersion curves with respect to each other for the three states are consistent with the asymmetric spectra shown in Figs. 5(a) and 5(b). For example, using bichromatic 2PPE at 267.5/535 nm, electrons are excited by the UV photon from the $n=0$ surface state to the $n=2$ image state at $k_{\|}\sim 0$; this same UV photon energy is also resonant between the $n=0$ and 1 states at ~17°. Thus for this UV wavelength resonant peaks are found for the $n=2$ and 1 states at 0° and 17°, respectively.

In addition to the changes in the dispersive behavior of the three surface states, small changes in the binding energy of three states were also measured. A ~50 meV upward shift in the energy band was measured for the $n=1$ state along with a ~70 meV upward shift for the $n=0$ state. However, no apparent shift was measured for the $n=2$ state. Also, a downward work function change was measured by comparing the low-energy cutoff shifts in the 1PPE spectra from the front, Cu(775), and back, Cu(111), sides of the same sample at higher photon energies ($h\nu \geq 4.4$ eV). The overall work function on stepped Cu(775) was seen lowered by ~40 meV as compared to that on flat Cu(111).

IV. DISCUSSION

A. Dispersion shifts in *k* space

The data displayed in Fig. 6 show that the electron dispersion curves have their minimum values at three different locations in $k_{\|}$ space. Such electronic behavior is very different from that on flat fcc surfaces for which the dispersion curves are nested about $k_{\|}=0$. To understand this behavior it is necessary to consider the formation of these surface-related states.

First, on a flat surface, image states are confined by an 1D Coulombic potential with the 2D image-state electron exhibiting free-electron-like motion in a plane parallel to its image plane. Hence, the position of the parabolic dispersion curve in k_1 space is determined by the image-plane orientation, i.e., the dispersion-band minimum occurs at the normal of the image plane. Calculations using the phase-accumulation method[14] show that the $n=1$ image state would have an average distance $l\sim 2$ Å above the image plane while the $n=2$ image-state electron would be ~12 Å above the surface.

On a stepped surface the interaction of an image electron with the surface is altered from that on a flat surface. First, charge smoothing at steps on a metal surface is known to lead to the formation of local step-edge dipoles[30] oriented perpendicular and outward from the edge. Second, the polarization of charge in the metal due to the image electron will also be perturbed by the steps. As a result of both effects, the image electron will no longer move in a simple one-dimensional potential. Further, the character of this potential will clearly depend on the distance of the electron from the surface plane. Because of the close proximity to the surface, the $n=1$ image-state electron may be expected to follow closely the local topography of the stepped surface. For example, based on classical electrostatics, the electric field of an electron located a distance $l=2$–3 Å above the surface would extend $\sim\sqrt{2}l$ to either side of its projected position on the substrate. Thus, a 14 Å-wide terrace would be sufficient to support a $n=1$ image state. In addition, the lifetime of the $n=1$ state on this surface is sufficiently short, e.g., ~8 fs even on flat Cu(111),[28,31] that for the small values of lateral momentum ($k_{\|}\leq 0.2$ Å^{-1}), perpendicular to the step considered here, an image-state electron will not, on average, transverse more than one terrace during its lifetime. As a result, its image plane will be that of a local (111) terrace instead of the general plane of the (775) surface. In fact, the dispersion data of the $n=1$ state shown in Fig. 6 agree well with this explanation. Specifically, the $n=1$ maximum binding energy is located at $k_{\|}\sim 0.09$ Å^{-1}, which corresponds to the terrace normal [111], instead of the surface normal at $k_{\|}=0$, thus showing that the $n=1$ state is oriented by the step terrace not the general surface plane of Cu(775).

On the other hand, the $n=2$ state is located much further ($l\sim 12$ Å) away from the surface and, thus, the lateral extent of its instantaneous image dipolar field at the surface will be averaged over at least two adjacent steps. Therefore, the $n=2$ state will have an image plane defined by the averaged Cu(775) surface and its dispersion curve will be oriented by the overall Cu(775) plane and not the individual step terrace in the [111] direction, i.e., the dispersion minimum occurs at $k_{\|}=0$, as shown by the data in Fig. 6. Hence, the 2D Coulombic potential is sampled at two characteristic distances from the surface: one at a dimension much smaller than the terrace width and one at dimensions greater than a terrace width.

Note also that the $n=1$ dispersion curve exhibits a shape which is not symmetrically parabolic and, in fact, appears to have a significant secondary minimum located at $k_{\|}=0$. This behavior suggests that the lateral motion of the $n=1$ image-state electron is not determined simply by a single (111) terrace direction, i.e., the $n=1$ dispersion is not obtained by a simple shifting of the free-electron-like dispersion curve

from $k_{\parallel}=0$ to $k_{\parallel}\sim 0.09\ \text{Å}^{-1}$ in going from Cu(111) to Cu(775). In fact, the steps on Cu(775) are asymmetric with respect to the surface normal. The effects of this asymmetry have been observed previously on stepped Cu(001),[8] where 2PPE signals in the $k_{\parallel}<0$ region were significantly weaker than in the $k_{\parallel}>0$ region. This phenomenon was attributed to different scattering efficiencies from the asymmetric step potential, depending on whether the image-state electron approached from the [112] or the [1 12] direction. On the stepped Cu(001), the excitation for the 2PPE process is from bulk continuum and thus the difference between electrons with $\pm k_{\parallel}$ is easily seen from the angle-dependent EDC at a fixed excitation wavelength. On stepped Cu(775), which requires resonant excitation, asymmetric scattering could be detected by comparing the relative magnitude of resonance signal on the opposite side of the SBZ center, $k_{\parallel}=0$ (or the surface normal). Because of this breaking of symmetry on Cu(775) due to the asymmetric steps, the final dispersion of $n=1$ is the result of a simple dispersion displacement due to orientation by the (111) terrace and the asymmetric dispersion behavior around $k_{\parallel}=0$ as the electron moves toward or away from the step riser.

Next, in order to understand the location of the dispersion minima for the $n=0$ crystal-induced state on Cu(775), it is necessary to examine the projection of the bulk band structure onto the 2D BZ for that specific surface. In the case of flat Cu(111), because the L neck of the bulk Fermi surface is orthogonal to the [111] direction, the bulk sp gap is projected onto the center of the hexagonal surface Brillouin zone, i.e., the center of the band gap is in the direction of [111], or at the $\bar{\Gamma}$ point in k space. Thus the $n=0$ band minimum is at $k_{\parallel}=0$ and its dispersion is symmetric about the surface normal. For Cu(775), the surface lattice structure is changed from the close-packed hexagon of Cu(111) to a nearly rectangular lattice consisting of ~ 7 atomic rows in the [1 10] and 2 atomic rows in the [112] direction. The 2D surface BZ is thus reduced by a factor of 6.3 from that on Cu(111) in the direction perpendicular to the step, giving reciprocal-lattice vectors of 1.22 and $0.44\ \text{Å}^{-1}$ along the [1 10] and [112] directions, respectively, as shown in Fig. 7. Because of this narrower surface BZ, even the relatively small tilt of the vicinal surface, with respect to Cu(111), causes the projection of the bulk L neck to fall on the boundary of the (775) BZ. In fact, the center of the projected sp gap is now at the boundary of the surface Brillouin zone in the [112] direction. The maximum binding energy of the $n=0$ surface state, supported by the band gap, occurs at the center of the gap, now at $k_{\parallel}\sim 0.22\ \text{Å}^{-1}$ instead of $k_{\parallel}=0$, which corresponds to the [775] direction (vicinal surface normal).

The measured dispersion data for $n=0$, in Fig. 6, indeed show the band minimum is at $k_{\parallel}\sim 0.22\ \text{Å}^{-1}$, detected at $\sim 19°$ from the surface normal, a direction clearly experimentally distinguishable from the terrace normal. This $k_{\parallel}$ value corresponds to the distance from the surface BZ center to the zone boundary along the [112] direction (perpendicular to the steps), in agreement with discussion presented above. Figure 6 also shows a similar downward dispersion away from the center for $k_{\parallel}<0$, i.e., in the [1 12] direction, indicating the dispersion is symmetric with respect to the zone center. In general, the presence of the asymmetric step-edge potential breaks the surface symmetry on Cu(775) and the dispersion of the $n=0$ surface state should not be symmetric about $k_{\parallel}=0$, in principle. The reason that the $n=0$ dispersion appears to be symmetric with respect to the zone center is because this surface state is very weakly localized to the surface, so that it is only weakly influenced by the surface step potential, in contrast to the physics for the $n=1$ state but similar to that for the $n=2$ state.

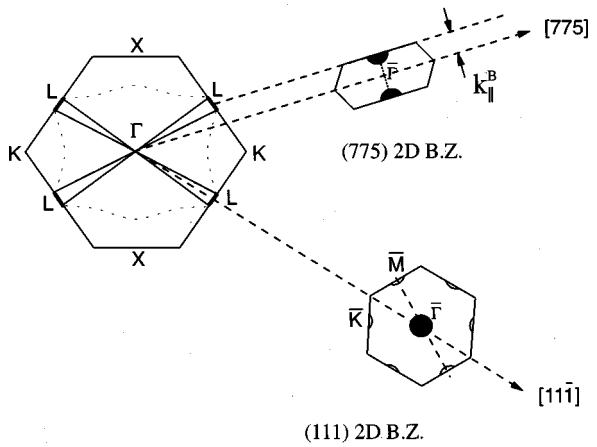

FIG. 7. A schematic drawing of the projection of the L neck onto the surface Brillouin zones for Cu(111) and Cu(775), after Ref. 10. The picture on the left is the cut profile through the 3D BZ of Cu for the relevant projection. The shaded areas in (111) and (775) SBZ's are the projected band gaps.

This band-gap-projection argument is also supported by the fact that similar behavior is seen, using occupied-state photoemission (i.e., 1PPE), for the dispersion curves of $n=0$ surface states on the vicinal surfaces of other noble metals[10] and for a different surface orientation of vicinal Cu.[11] For example, photoemission experiments by Shapiro, Miller, and Chiang[11] showed that on stepped Cu(332), the minimum in the dispersion curve of the same sp surface state as examined here was seen at 7° from the surface normal. This angle did not correspond to the change from flat (111) expected on the basis of a simple tilt of the (111) terraces on the vicinal surface,[9] which would have given a dispersion minimum at $\sim 10°$. Instead, the measured angle of 7° was attributed to the fact that the orientation of the dispersion in k space of this crystal-induced state resulted from the projection of the bulk band structure (more specifically the band gap) on that particular surface. For our surface measured with resonant 2PPE, much lower photon energies were used. As a result, the distinction between the terrace tilt angle and the dispersion minimum was much clearer, namely, the dispersion minimum occurred at $\sim 19°$ in comparison with the tilt of the terrace normal at 8–9°.

In summary, based on the dispersion properties of the $n=0$, 1, and 2 states, it is clear that the $n=2$ image state is oriented by the overall surface plane while the $n=1$ image state is oriented by the local terrace plane, with the difference in the two states reflecting their different heights above the surface. The $n=0$ surface state, which has an average distance of ~ 4 Å beneath the surface,[32] has its dispersion minima determined by the surface Brillouin zone on

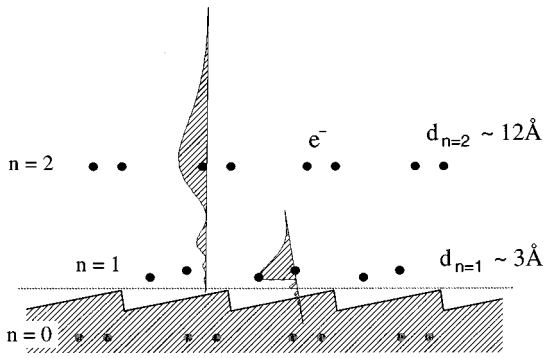

FIG. 8. A schematic of the position and orientation for the $n=1$ and 2 image states at stepped Cu(775). The average distances from the surface are ~3 and ~12 Å for the $n=1$ and 2 states, respectively.

Cu(775). The height dependence of the surface and image states is summarized in Fig. 8.

B. Binding energy shifts on the $n=0$, 1, 2 states

The presence of periodic surface potentials associated with a step array might be expected to shift the binding energies of surface electrons. As mentioned in Sec. III, in fact, in our experiments on the stepped surface upward shifts in the binding energies for both the surface ($n=0$) and image state ($n=1$) were observed as well as a reduction in the surface work function, all in comparison to their values on the corresponding flat surface. The work-function reduction is in accord with the formation of local dipoles due to charge smearing at the step edge. The reduction measured on this surface is local in nature since it results from the local electronic structure change at the step edge. Local work-function changes have recently been investigated extensively on single-crystal metal surfaces for a variety of surface conditions.[8,15] On the larger planar areas of the step terraces, which support the $n=1$ image state, as discussed in the previous section, the work function would remain virtually the same as on flat Cu(111). As a result, a step-induced local work-function change does not contribute to the binding-energy shift in the $n=1$ image state. This point is also evident from the fact that the work-function changes in the opposite direction to the shift in the image state (i.e., the image state shifts upwards in energy while the surface work function decreases), Since the image state is known to be pinned to the local vacuum level,[33] any reduction in the work function on the terrace would cause a decrease in the binding energy. Because this is contrary to our observation, another explanation must be sought.

In order to understand such binding-energy shifts for both crystal-and image-induced surface states in going from a flat Cu(111) to the Cu(775) surface, the phase-analysis model, introduced by Echenique and Pendry[34] and further developed by Smith,[14] is used. Adopting the nomenclature of Ref. 34, bound surface states appear in a multiple-reflection model when the following phase condition is satisfied:

$$\Phi=\Phi_B+\Phi_C=2\pi n, \tag{1}$$

where Φ_B and Φ_C denote the phase changes related to surface barrier and crystal barrier, respectively. For the barrier-induced image states ($n=1,2$), the dominant factor in the binding energy is due to the rapid variation of Φ_B and hence the surface potential.[14] On a flat metal surface, $\partial\Phi_B/\partial E$ results from the turning point phase shift at the Coulombic-like potential barrier, which acts perpendicular to the surface.[34] The electron is thus confined vertically. On structural or heterogeneous surfaces, there are, as mentioned above, lateral potential gradients which may shift the binding energy. For example, Fischer, Fauster, and Steinmann[15] have reported lateral confinement shifts in image electron binding energies confined by islands <100 Å in diameter. In the present experiments step-edge potentials may also confine electrons.[35] The influence of the step discontinuity on electrons at different heights from the step can be estimated from a calculation of the electrostatic potential induced by the dipolelike charge-density formation at the step edge. In the calculation, a jellium model for the positive charge background with the step structure of Cu(775) was used along with the electron-density profile determined by minimizing the surface energy using local-density expressions.[30] The electron density are expressed as follows,

$$\rho(\mathbf{r})=\rho_0[S(\beta[z-hS(\gamma x)])+1/2], \tag{2}$$

where $\boldsymbol{r}=\boldsymbol{r}(x,y,z)$, $S[x]=-\mathrm{erf}[x]/2$, ρ_0 is the electron density far inside the bulk lattice, the step height $h=3.9$, and the falloff parameters $\beta=0.49$ and $\gamma=0.6$ for the electron-density spill over the rigid positive charge ledge on the stepped copper surface in z, normal to the step terrace, and x, and perpendicular to z and the step, respectively (all in atomic units, as is in the following expression). The electrostatic potential due to this charge distribution is then given by[30]

$$V(x,z)=-2\int\int \ln\left\{\frac{|r-r'|}{|r_0-r'|}\right\}\rho(r')dx'dz', \tag{3}$$

where r_0 is the reference point at the step for zero potential and $r=r(x,z)$.

For Cu(775), the step potential was found to be most effective within ±2 Å of the plane through the middle of the step corrugation and in the direction perpendicular to the step terrace and to diminish rapidly away above the step, as shown in Fig. 9. At a distance of 12 Å above the surface, the potential change along the x plane induced by the step edge is small, less than 2% of the maximum variation at $z=0$, and hence has no appreciable effect on the $n=2$ electron. This result is in accord with the lack of binding-energy shift seen in our measurements; however, for the $n=1$ electron, the upward shifts in energy can be explained by the partial confinement resulting from the step potential formed at the step edge.

In order to estimate the binding-energy change due to electron confinement by the step-edge potential discontinuities, a 1D Kronig-Penney model was solved numerically for a variety of trial potentials; this numerical approach provides a flexible method for examining the effects of these trial potentials on the electron dispersion near the surface. The analysis considered simple square-wave potentials as well as bipolar rectangular potentials with various potential widths and heights. For example, the simulation, using a square step potential with 0.4-V height, 3-Å width and a 14-Å pe-

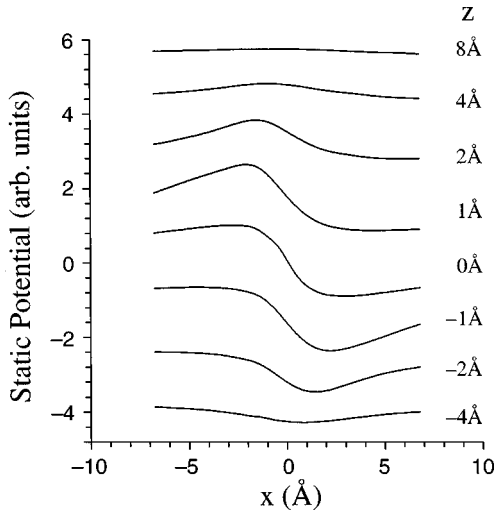

FIG. 9. Calculated step potentials as a function of height above and below the step.

riod, yielded a 50-meV energy shift of the $n=1$ band bottom towards the vacuum level. Thus binding-energy shifts close to the values measured in our resonant 2PPE experiment can readily be obtained with reasonable periodic step potentials. For the $n=2$ image state, realistic estimates of the potential using the calculation for $V(x,z)$ described above showed no detectable change in binding energy; a result in agreement with our measurements. These results suggest that the $n=2$ state is not strongly affected by the step potential because the step potential perturbation is negligible at $z\sim 12$ Å above the surface for the maximum probability density of the $n=2$ state.

In contrast to the lack of previous measurements of energy shifts to the $n=1$ state, there have been several previous measurements[7,11] for the $n=0$ surface state at stepped surfaces. For example, Sanchez *et al.*[7] have performed STM and photoemission measurements on several stepped copper surfaces and observed a shift in the binding energy which increased with decreasing terrace width. This shift was attributed to the confinement of $n=0$ electrons by the step potential.

The $n=0$ surface state can be categorized as crystal-induced because the solution exists due to rapid variation of the crystal-induced phase change Φ_C at an energetic position close to the bottom of the projected band gap, where the variation of Φ_B makes an insignificant contribution to the phase requirement of Eq. (1); in fact, previous calculations have shown that the position of the surface state ($n=0$) is relatively insensitive to any specific form for the surface barrier.[14] Since the $n=0$ state is determined by the crystal-phase change, chiefly through the band-gap parameter V_g,[14] shifts in the binding energy of this sp surface state can easily occur through any alteration in the surface band structure. For example, Schneider *et al.*[36] performed a series of high-resolution angle-resolved photoemission spectroscopy measurements on the (111) surfaces of Ag, Au, and Cu as a function of the surface temperature, where the energy shifts have been attributed to band-gap shifting. Subsequently, Paniago *et al.*[37] showed, by calculating the effects of the V_g change on Φ_C, that the shift of L_2 gave rise to a shift of the $n=0$ surface state on Cu(111) in the same direction. In a related temperature-dependence experiment they also showed that the $n=0$ state shifted upwards in proportion to the shift of the bulk band gap that resulted from the temperature increase. Note, however, that this same temperature dependence of the crystal band structure does not lead to binding-energy shifts in the $n=1$ image state, as demonstrated by Wu *et al.*,[33] because the $n=1$ is considerably decoupled from the surface structure and its binding energy is primarily affected by the barrier potential.

Thus, for the case of stepped copper surfaces, the $n=0$ surface state would be expected to shift due to similar changes in the projected band structure onto the specific surface. Such an effect of changes in the projected band structure is seen clearly in an extreme case by the change in the location of the $n=0$ state for different copper surfaces. For example, on Cu(100), the L gap is projected to X and the subsequent surface band gap has a cusp on the lower band edge at X, instead of a smooth parabolic shape as on Cu(111).[17,36] Consequently, the induced sp surface state due to this band gap was found to be just 0.06 eV below the Fermi level,[38] a upward shift of over 0.3 eV compared to the same state on Cu(111). Changes in V_g could have similar consequences on the $n=0$ state due to the projected band structure on different stepped surfaces. For the case of Cu(775), a careful calculation of the projection of the bulk band onto the (775) 2D Brillouin zone must be done before the surface band structure of this surface can be determined accurately or the effect of this structure on the binding energy of the crystal-induced $n=0$ state can be evaluated. At this time, more precise theoretical work is needed to determine whether the shifts observed by us are due to the changes in the projected band structure on the (775) surface or to the direct influence on the $n=0$ electron by the step potential which can also lead to an upward shift observed in the measurement based on simple K-P analyses.

V. CONCLUSIONS

In summary, a comparison of the dispersion curves of these surface or near-surface electrons, as measured in our experiments, reveals a different electronic response to the stepped surface, which can be related to their distances from the surface plane. Specifically, the symmetry in the energy dispersion of the $n=0$ surface state and the $n=1$ image state about the surface normal was lost on the stepped Cu(775) as compared to the planar Cu(111). In fact the minimum in the dispersion curve of the $n=1$ image state, a state which exists 2–3 Å above the surface, was measured to be oriented about the local normal of the (111) terrace on the stepped Cu(775). However, the $n=2$ state, located further above the surface, was found to disperse about the normal of the (775) surface plane. Finally, the electronic structure of the embedded sp-like surface state appeared not to be dependent on the (111) terrace orientation nor the (775) surface plane, but instead was determined by the projection of the bulk band structure on the (775) surface.

More recently, in connection with the experiments described above, monochromatic UV 2PPE experiments enabling a wider-angle detection range, have also showed that the step potential induced at the step edge is sufficiently strong for the $n=1$ electron to give rise to consistent um-

klapp processes at several different photon energies. In particular, the measurements showed different amplitudes for the oscillatory dispersion at different photon energies for the $n=1$ image-state electrons; the period of this oscillation was 0.44 $Å^{-1}$, suggesting a transformation in k space by the step reciprocal-lattice vector of the same value. As suggested in the introduction as well as in the potential calculations in the previous section, the step potential should be of sufficient magnitude to reflect electrons in a direction perpendicular to the steps. This process should be sufficiently strong to cause zone folding of the surface electron dispersion curve and cause umklapp transitions on surface electrons. Such an effect has recently been reported for $n=1$ electrons on Cu(001). Note that such behavior has not been seen in the case of electrons in the crystal-induced $n=0$ surface states on stepped surfaces,[11] which is consistent with the surface-state delocalization in the surface plane as discussed in Sec. IV. Details of these measurements will be presented elsewhere.

ACKNOWLEDGMENTS

We gratefully acknowledge support from the Army Research Office Contract No. DAAH04-95-G-0535, Joint Services Electronics Program Contract No. DAAH04-94-G-0057, and the National Science Foundation Contract No. ECS-94-24252. We would like to thank Feng Huang for his assistance in the step potential calculation. We are indebted to Professor Zhen Wu, Dr. Jerry Tersoff, and Dr. Norton Lang for extensive and critical discussions of the results presented here.

[1] M. F. Crommie, C. P. Lutz, and D. M. Eigler, Nature (London) **363**, 524 (1993); Science **262**, 218 (1993).
[2] Y. Hasegawa and Ph. Avouris, Phys. Rev. Lett. **71**, 1071 (1993).
[3] J. E. Ortega, F. J. Himpsel, R. Haight, and D. R. Peale, Phys. Rev. B **49**, 13 859 (1994).
[4] Ph. Avouris and I.-W. Lyo, Science **264**, 942 (1994).
[5] S. Crampin, M. H. Boon, and J. E. Ingelsfield, Phys. Rev. Lett. **73**, 1015 (1994).
[6] T. Jung, R. Schlittler, J. K. Gimzewski, and F. J. Himpsel, Appl. Phys. A **61**, 467 (1995).
[7] O. Sanchez, J. M. Garcia, P. Segovia, J. Alvarez, A. L. Vazquez de Parga, J. E. Ortega, M. Prietsch, and R. Miranda, Phys. Rev. B **52**, 7894 (1995); J. M. Garcia, O. Sanchez, P. Segovia, J. E. Ortega, J. Alvarez, A. L. Vazquez de Parga, and R. Miranda, Appl. Phys. A **61**, 609 (1995).
[8] X. Y. Wang, X. J. Shen, and R. M. Osgood, Jr., R. Haight, and F. J. Himpsel, Phys. Rev. B **53**, 15 738 (1996).
[9] R. S. Williams, P. S. Wehner, S. D. Kevan, R. F. Davis, and D. A. Shirley, Phys. Rev. Lett. **41**, 323 (1978).
[10] P. Heimann, H. Miosga, and H. Neddermeyer, Phys. Rev. Lett. **42**, 801 (1979).
[11] A. P. Shapiro, T. Miller, and T.-C. Chiang, Phys. Rev. B **38**, 1779 (1988).
[12] R. F. Davis, R. S. Williams, S. D. Kevan, P. S. Wehner, and D. A. Shirley, Phys. Rev. B **31**, 1997 (1985).
[13] N. V. Smith, Rep. Prog. Phys. **51**, 1227 (1988).
[14] N. V. Smith, Phys. Rev. B **32**, 3549 (1985).
[15] R. Fischer, Th. Fauster, and W. Steinmann, Phys. Rev. B **48**, 15 496 (1993).
[16] P. O. Gartland and B. J. Slagsvold, Phys. Rev. B **12**, 4047 (1975).
[17] S. D. Kevan, Phys. Rev. Lett. **50**, 526 (1983).
[18] G. D. Kubiak, Surf. Sci. **201**, L475 (1988).
[19] Th. Fauster and W. Steinmann, in *Photonic Probes of Surfaces*, edited by P. Halevi (Elsevier, Amsterdam, 1995).
[20] S. Schuppler, N. Fischer, W. Steinmann, R. Schneider, and E. Bertel, Phys. Rev. B **42**, 9403 (1990).
[21] H. Wagner, in *Solid Surface Physics*, edited by J. Holzl, F. K. Schulte, and H. Wagner, Springer Tracts in Modern Physics Vol. 85 (Springer-Verlag, Berlin 1979), p. 151–221.
[22] T. L. Gilton, J. P. Cowin, D. Kubiak, and A. V. Hamza, J. Appl. Phys. **68**, 4802 (1990).
[23] S. Schuppler, N. Fischer, Th. Fauster, and W. Steinmann, Appl. Phys. A **51**, 322 (1990).
[24] R. Shakeshaft and L. Spruch, Phys. Rev. B **31**, 1535 (1985).
[25] K. Giesen, F. Hage, F. J. Himpsel, H. J. Riess, W. Steinmann, and N. V. Smith, Phys. Rev. B **35**, 975 (1987).
[26] W. Steinmann, Appl. Phys. A **49**, 365 (1989).
[27] B. Quiniou, V. Bulovic, and R. M. Osgood, Jr., Phys. Rev. B **47**, 15 890 (1993).
[28] T. Hertel, E. Knoesel, M. Wolf, and G. Ertl, Phys. Rev. Lett. **76**, 535 (1996).
[29] R. Haight, Surf. Sci. Rep. **21**, 277 (1995).
[30] M. D. Thompson and H. B. Huntington, Surf. Sci. **116**, 522 (1982).
[31] W. Wallauer and Th. Fauster, Surf. Sci. **374**, 44 (1997).
[32] M. Weinert, S. L. Hulbert, and P. D. Johnson, Phys. Rev. Lett. **55**, 2055 (1985).
[33] Z. Wu, B. Quiniou, J. Wang, and R. M. Osgood, Jr., Phys. Rev. B **45**, 9406 (1992).
[34] P. M. Echenique and J. B. Pendry, J. Phys. C **11**, 2065 (1978).
[35] Notice that, for simplicity, in the discussion that follows only the ''built-in'' or static potential gradients in the near-surface potential are discussed. As mentioned earlier the steps would also be expected to change the surface polarization by the image charge—again introducing a lateral component. We assume without proof that the static effects are more important.
[36] R. Schneider, H. Dürr, Th. Fauster, and V. Dose, Phys. Rev. B **42**, 1638 (1990).
[37] R. Paniago, R. Matzdorf, G. Meister, and A. Goldmann, Surf. Sci. **336**, 113 (1995).
[38] S. D. Kevan, Phys. Rev. B **28**, 2268 (1983).